Hindawi Publishing Corporation
Shock and Vibration
Volume 2014, Article ID 405421, 10 pages
http://dx.doi.org/10.1155/2014/405421

Research Article

Semiactive Vibration Control Using a Magnetorheological Damper and a Magnetorheological Elastomer Based on the Bouc-Wen Model

Wei Zhu and Xiao-ting Rui

Institute of Launch Dynamics, Nanjing University of Science and Technology, Nanjing 210094, China

Correspondence should be addressed to Wei Zhu; zhuwei@cqu.edu.cn

Received 10 April 2014; Revised 21 May 2014; Accepted 24 May 2014; Published 15 June 2014

Academic Editor: Ahmet S. Yigit

A vibration control system is put forward using a magnetorheological damper (MRD) and a magnetorheological elastomer (MRE) connected in series. In order to model the hysteresis of the MRD, a Bouc-Wen model and a corresponding parameter identification method are developed for the MRD. The experimental results validate the proposed Bouc-Wen model that can predict the hysteretic behavior of the MRD accurately. The role of the MRE is illustrated by an example of a single degree-of-freedom system. A semiactive vibration control strategy of the proposed vibration control system is proposed. To validate this new approach, experiments are conducted and the results highlight significantly improved vibration reduction effect of the proposed vibration control system than the vibration control system only using the MRD.

1. Introduction

Magnetorheological dampers (MRDs) hold promise for vibration control since their properties can be adjusted in real time, and unlike active devices they do not inject energy into the system being controlled and have relatively low power requirements. The MRDs, using MR fluids that exhibit controllable yield characteristics, produces sizeable damping force for small input current. Being an energy dissipation device that cannot add mechanical energy to the structural system, an MR damper is also very stable and fail safe. MR fluid contains a suspension of iron particles in a carrier fluid such as oil [1].

The Bouc-Wen model [2] describes the hysteretic behavior of MR dampers except near small velocities. This shortcoming was rectified by Spencer et al. [3] in their modified Bouc-Wen model, where in additional damping and stiffness elements were used to model the low-velocity behavior and the accumulator, respectively, and voltage dependent parameters were introduced. Dominguez et al. [4] developed a current-frequency-amplitude dependent Bouc-Wen model and an identification method. Other damper models include the phase-transition model of Wang and Kamath [5] and modified LuGre friction model of Jiménez and Álvarez-Icaza [6] and Sakai et al. [7].

Various controller designs have been used with MR dampers. Predicting the applied voltage that produces a desired damper force is difficult due to the noninvertible force-voltage dynamics. Hence, different voltage laws have been considered. Xu and Shen [8] used bistate control strategies with a Bingham damper model, on-off current law, and neural network response prediction. Dyke et al. [9] implemented acceleration feedback linear quadratic Gaussian (LQG) control, using the modified Bouc-Wen model, to obtain the desired optimal damper force using measured accelerations, displacements, and damper force. Based on the classical sky-hook damping a novel semiactive control strategy, well suited for use in drive systems, is presented by Frey et al. [10]. Prabakar et al. [11] applied a half car model for simulating the semiactive suspension system. They modeled the parameters of a MRD by the modified Bouc-Wen model and determined that they fit the hysteretic behavior and put forward optimal semiactive preview control. Weber [12] presented a Bouc-Wen model-based control scheme which allows tracking the desired control force in real-time with

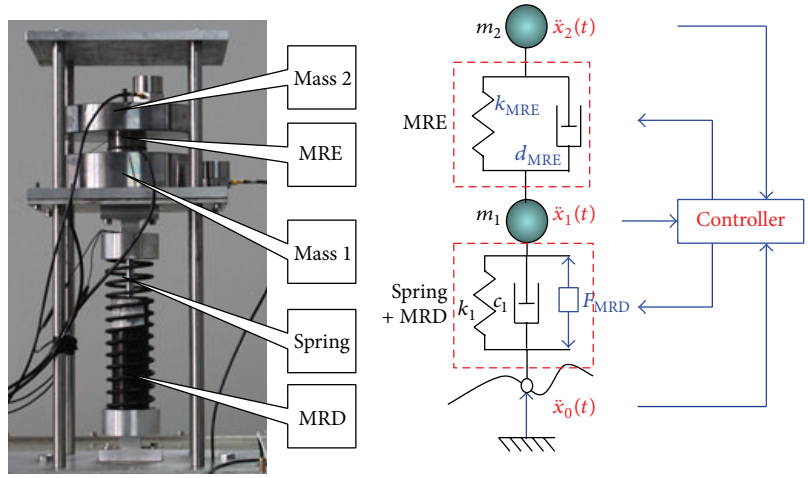

(a) Photograph (b) Schematic diagram

Figure 1: Vibration control system.

magnetorheological (MR) dampers without feedback from a force sensor.

However, the MRD can only change its damping and the response time is generally slower than 20 ms which could make the high-frequency performance of the vibration control system decrease [9].

Magnetorheological elastomers (MREs), like MR fluids, exploit magnetic forces between dispersed micron-sized ferromagnetic particles to produce a material with instantaneously adjustable properties. However in MR fluids the particles are dispersed within a liquid and operate in a postyield regime, while in MREs the particles are part of a structured elastomer matrix in a preyield regime [13]. Rigbi did the earliest work with what could be considered MRE materials but dealt mainly with the magnetic properties of a strained isotropic sample [14]. Jolly after considerable experience with MR fluids developed an anisotropic MRE, where spherical iron particles were aligned by an external magnetic field into long parallel chains within the curing rubber [15]. MREs can be used to make up for the shortcomings of MRDs in vibration control system due to the adjustable properties of their stiffness.

The paper is organized as follows. Section 1 contains a brief introduction, literature review, and aims and scope of the paper; Section 2 describes a vibration control device using a MRD and a MRE connected in series; Section 3 describes the Bocu-Wen model and parameter identification method for MRDs; a MRE device is put forward in Section 4; a semiactive vibration control strategy is proposed in Section 5; Section 6 presents experimental results and discussions, including comparisons with available results; and Section 7 contains the conclusions and future scope.

2. Vibration Control System

Figure 1 shows a vibration control system using a MRD and a MRE connected in series. In the design, the MRD is used to reduce the large-range and low-frequency vibration; the MRE is used to reduce the small-range and high-frequency vibration.

The dynamic equation of the vibration control device can be given by

$$\mathbf{M}\ddot{\mathbf{x}} + \mathbf{D}\dot{\mathbf{x}} + \mathbf{K}\mathbf{x} = \mathbf{\Gamma} f_{MRD} + \mathbf{K}_0\mathbf{x}_0, \tag{1}$$

where $\mathbf{x} = \begin{bmatrix} x_1 \\ x_2 \end{bmatrix}$. The system matrices are

$$\mathbf{M} = \begin{bmatrix} m_1 & 0 \\ 0 & m_2 \end{bmatrix}, \quad \mathbf{D} = \begin{bmatrix} d_{MRE} & -d_{MRE} \\ -d_{MRE} & d_{MRE} \end{bmatrix},$$
$$\mathbf{K} = \begin{bmatrix} k_1 + k_{MRE} & -k_{MRE} \\ 0 & k_{MRE} \end{bmatrix}, \quad \mathbf{\Gamma} = \begin{bmatrix} -1 \\ 0 \end{bmatrix}, \tag{2}$$
$$\mathbf{K}_0 = \begin{bmatrix} k_1 & c_1 \\ 0 & 0 \end{bmatrix}, \quad \mathbf{x}_0 = \begin{bmatrix} x_0 \\ \dot{x}_0 \end{bmatrix}$$

where f_{MRD} is the force of the MRD; k_{MRE} and c_{MRE} are the stiffness and viscous damping coefficient, respectively.

3. MRDs

3.1. Bouc-Wen Model of MRDs. In order to control the force of the MRD, it is essential to propose a model for MRDs. The Bouc-Wen model of MRDs is given by [1]

$$f_{MRD} = c(i)\dot{x} + k(i)(x - x_0) + \alpha(i)z$$
$$\dot{z} = A\dot{x} - \beta\dot{x}|z|^n - \gamma|\dot{x}||z|^{n-1}z, \tag{3}$$

where x and $\dot{x}$ are the damper displacement and velocity; z is the Bouc-Wen hysteresis operator; "$\cdot$" at the top of variables represents the first order derivative of the variables with respect to time; i is the current applied to the MRD; $k(i)$ and $c(i)$ are the stiffness and damping function of the efficient current, respectively; $\alpha(i)$ is function related to the MR material yield stress; x_0 is the initial displacement which

can be measured; A, β, γ, and n are the parameters of the Bouc-Wen hysteresis operator.

Let $h = \alpha z$. h is the hysteresis force. Equation (3) can be rewritten as

$$f_{\mathrm{MRD}} = c(i)\dot{x} + k(i)(x - x_0) + h, \tag{4}$$

$$\dot{h} = A(i)\dot{x} - \beta(i)\dot{x}|h|^n - \gamma(i)|\dot{x}|\,|h|^{n-1}h. \tag{5}$$

In order to use the Bouc-Wen model given by (4) and (5) to simulate the hysteretic behaviour of the MRD, the functions $c(i)$, $k(i)$, $A(i)$, $\beta(i)$, and $\gamma(i)$ and the parameters x_0 and n need to be identified.

3.2. Parameter Identification Method. The initial displacement x_0 can be obtained by measuring the displacement of the rod. Let the current i be a constant. The functions $c(i)$, $k(i)$, $A(i)$, $\beta(i)$, and $\gamma(i)$ are the constants c, k, A, β, and γ, respectively. Consider the corresponding forces $F_x(t)$ and $F_y(t)$ from the MRD with two periodical displacements $x(t)$ and $y(t)$, which are related by

$$y(t) = x(t) + q, \tag{6}$$

where q is a constant. We have

$$F_x(t) = c\dot{x}(t) + kx(t) + h_x(t), \tag{7}$$

$$F_y(t) = c\dot{x}_1(t) + k[x_1(t) + q] + h_y(t), \tag{8}$$

where $h_x(t)$ and $h_y(t)$ are the hysteresis force. According to (5) and (6), $h_x(t) = h_y(t)$.

Consider a set of N_1 points $(x_1, F_{x1}), \ldots, (x_j, F_{xj}), \ldots, (x_{N_1}, F_{xN_1})$ in the hysteresis curve force $F_x(t)$ against displacement $x(t)$ determined by (7) and $(y_1, F_{y1}), \ldots, (y_j, F_{yj}), \ldots, (y_{N_1}, F_{yN_1})$ in the hysteresis curve force $F_y(t)$ against displacement $y(t)$ determined by (8). With the least-squares method, the parameter k is given by

$$k = \frac{\sum_{j=1}^{N_1}\left(F_{yj} - F_{xj}\right)}{N_1 q}. \tag{9}$$

The Bouc-Wen hysteresis operator given by (5) possesses the symmetrical characteristic [17, 18]. Therefore, we have [19]

$$\begin{aligned} F_{xj}(\min) + F_{xj}(\max) = {} & c\left(\dot{x}_j(\min) + \dot{x}_j(\max)\right) \\ & + k\left(x_j(\min) + x_j(\max)\right), \end{aligned} \tag{10}$$

where $x(\min)$ and $x(\max)$ are the minimum and maximum value of the displacement x in the jth ($j = 1, 2, \ldots, N_2$) period, respectively; $F_{xj}(\min)$ and $F_{xj}(\max)$ are corresponding force; $\dot{x}_j(\min)$ and $\dot{x}_j(\max)$ are corresponding velocity.

With the least-squares method, the parameter c can be given by

$$c = \frac{1}{N_2}\sum_{j=1}^{N_2}\frac{F_{xj}(\min) + F_{xj}(\max) - k\left(x_j(\min) + x_j(\max)\right)}{\dot{x}_j(\min) + \dot{x}_j(\max)}. \tag{11}$$

According to (6), we have

$$\frac{\mathrm{d}h_x}{\mathrm{d}x} = A - [\gamma + \beta\,\mathrm{sgn}(\dot{x}h_x)]\,|h_x|^n, \tag{12}$$

where

$$\mathrm{sgn}(x) = \begin{cases} 1, & x \geq 0, \\ -1, & x < 0. \end{cases} \tag{13}$$

According to (4), the hysteresis operator can be written as

$$h_x = F_x - kx - c\dot{x}. \tag{14}$$

Let $h_x = 0$. According to (14), we have

$$F_x - kx - c\dot{x} = 0. \tag{15}$$

Assume that (x_*, F_*) is the solution of (15). According to (12) and (14), we have

$$A = \left.\frac{\mathrm{d}h_x}{\mathrm{d}x}\right|_{x=x_*} = \left.\frac{\mathrm{d}F_x}{\mathrm{d}x}\right|_{u=u_*} - k_v - c\frac{1}{\mathrm{d}t}. \tag{16}$$

When $\dot{x}(t) > 0$, consider a set of points $x_1, \ldots, x_j, \ldots, x_N$ ($j = 1, 2, \ldots, N_3$) in $x(t)$, which ensures that the corresponding hysteresis displacement $h_1, \ldots, h_j, \ldots, h_{N3}$ is larger than zero. Then (12) can be rewritten as

$$\begin{aligned} \left.\frac{\mathrm{d}h}{\mathrm{d}x}\right|_{x=x_1} &= A - (\beta + \gamma)h_1^n \\ &\vdots \\ \left.\frac{\mathrm{d}h}{\mathrm{d}x}\right|_{x=x_j} &= A - (\beta + \gamma)h_j^n \\ &\vdots \\ \left.\frac{\mathrm{d}h}{\mathrm{d}x}\right|_{x=x_{N_3}} &= A - (\beta + \gamma)h_{N_3}^n. \end{aligned} \tag{17}$$

Let $-(\beta + \gamma) > 0$. According to (17), we have

$$\begin{aligned} \ln\left(\left.\frac{\mathrm{d}h}{\mathrm{d}x}\right|_{x=x_1} - A\right) &= n\ln h_1 + \ln[-(\beta + \gamma)] \\ &\vdots \\ \ln\left(\left.\frac{\mathrm{d}h}{\mathrm{d}x}\right|_{x=x_j} - A\right) &= n\ln h_j + \ln[-(\beta + \gamma)] \\ &\vdots \\ \ln\left(\left.\frac{\mathrm{d}h}{\mathrm{d}x}\right|_{u=u_{N_3}} - A\right) &= n\ln h_{N_3} + \ln[-(\beta + \gamma)]. \end{aligned} \tag{18}$$

According to (18) and the least-squares method, we have

$$n = \left(N_3 \sum_{j=1}^{N_3} \ln h_j \ln \left(\left. \frac{dh}{dx} \right|_{x=x_j} - A \right) - \sum_{j=1}^{N_3} \ln h_j \sum_{j=1}^{N_3} \ln \left(\left. \frac{dh}{dx} \right|_{x=x_j} - A \right) \right) \times \left(N_3 \sum_{j=1}^{N_3} (\ln h_j)^2 - \left(\sum_{j=1}^{N_3} \ln h_j \right)^2 \right)^{-1}, \tag{19}$$

$$\beta + \gamma = \left[-\exp \left(\sum_{j=1}^{N_3} \ln \left(\left. \frac{dh}{dx} \right|_{x=x_j} - A \right) - n \sum_{j=1}^{N_3} \ln h_j \right) \times (N_3)^{-1} \right]. \tag{20}$$

When $\dot{x}(t) < 0$, consider a set of points $x_{N_3+1}, \ldots, u_{N_3+j}, \ldots, x_{2N_3}$ $(j = 1, 2, \ldots, N)$ in $x(t)$, which ensures that the corresponding hysteresis displacement $h_{N+1}, \ldots, h_{N+j}, \ldots, h_{2N}$ is larger than zero. Then (12) can be rewritten as

$$\begin{aligned} \left. \frac{dh}{dx} \right|_{u=u_{N_3+1}} &= A - (-\beta + \gamma) h_{N_3+1}^n \\ &\vdots \\ \left. \frac{dh}{dx} \right|_{u=u_{N_3+j}} &= A - (-\beta + \gamma) h_{N_3+j}^n \\ &\vdots \\ \left. \frac{dh}{dx} \right|_{x=x_{2N_3}} &= A - (-\beta + \gamma) h_{2N_3}^n. \end{aligned} \tag{21}$$

Let $\beta - \gamma > 0$. According to (21), we have

$$\begin{aligned} \ln \left(\left. \frac{dh}{dx} \right|_{x=x_{N_3+1}} - A \right) &= n \ln h_{N_3+1} + \ln (\beta - \gamma) \\ &\vdots \\ \ln \left(\left. \frac{dh}{dx} \right|_{x=x_{N_3+j}} - A \right) &= n \ln h_{N_3+j} + \ln (\beta - \gamma) \\ &\vdots \\ \ln \left(\left. \frac{dh}{dx} \right|_{x=x_{2N_3}} - A \right) &= n \ln h_{2N_3} + \ln (\beta - \gamma). \end{aligned} \tag{22}$$

With the least-squares method, (22) can be rewritten as

$$\beta - \gamma = \exp \left[\left(\sum_{j=1}^{N_3} \ln \left(\left. \frac{dh}{dx} \right|_{x=x_{N_3+j}} - A \right) - n \sum_{j=1}^{N_3} \ln h_{N_3+j} \right) \times (N_3)^{-1} \right]. \tag{23}$$

According to (20) and (23), the parameters β and γ are given by

$$\begin{aligned} \beta = \frac{1}{2} \Bigg\{ & -\exp \left[\left(\sum_{j=1}^{N_3} \ln \left(\left. \frac{dh}{dx} \right|_{x=x_j} - A \right) - n \sum_{j=1}^{N_3} \ln h_j \right) \times (N_3)^{-1} \right] \\ & + \exp \left[\left(\sum_{j=1}^{N_3} \ln \left(\left. \frac{dh}{dx} \right|_{x=x_{N_3+j}} - A \right) - n \sum_{j=1}^{N_3} \ln h_{N_3+j} \right) (N_3)^{-1} \right] \Bigg\}, \\ \gamma = -\frac{1}{2} \Bigg\{ & \exp \left[\left(\sum_{j=1}^{N_3} \ln \left(\left. \frac{dh}{dx} \right|_{x=x_j} - A \right) - n \sum_{j=1}^{N_3} \ln h_j \right) \times (N_3)^{-1} \right] \\ & + \exp \left[\left(\sum_{j=1}^{N_3} \ln \left(\left. \frac{dh}{dx} \right|_{x=x_{N_3+j}} - A \right) - n \sum_{j=1}^{N_3} \ln h_{N_3+j} \right) (N_3)^{-1} \right] \Bigg\}. \end{aligned} \tag{24}$$

According to (9), (11), (16), (19), and (24), under the single current, the parameters k, c, A, β, γ, and n can be identified if the periodical displacements $x(t)$ and $y(t)$

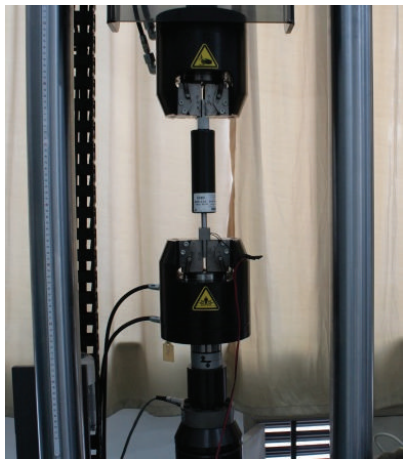

Figure 2: Photograph of the test setup.

and the corresponding forces $x(t)$ and $y(t)$ are known. Applying the various currents to the MRD, the corresponding parameters k, c, A, β, and γ can be obtained. With the least-squares method, the functions $c(i)$, $k(i)$, $A(i)$, $\beta(i)$, and $\gamma(i)$ can be identified.

3.3. Modeling Results. The MRD is subjected to sinusoidal excitations on an electrohydraulic servo fatigue machine (type: LFV 150 kN, the W + B GmbH, Switzerland) to validate the Bouc-Wen model and the corresponding parameter identification method. The primary components of the test setup are shown in Figure 1. The fatigue machine has its own software to collect the data from the data card and use them to plot force versus displacement and force versus velocity graphs for each test. A programmable power (type IT6122, the ITECH Electronic Co, Ltd) supply is used to feed current to the MRD. The damper is fixed to the machine via grippers as shown in the Figure 2. The machine excites the damper's piston rod sinusoidally, while a load cell measures the force on the damper and a linear variable displacement transducer measures the displacement of the piston rod as well as the relative velocity. Since the identification method uses the values of the derivatives at some points of the experimental data, it is necessary to filter the data before applying the identification algorithm. To this end, a second order filter of the form $\omega_n^2/(s^2 + 2\xi\omega_n + \omega_n^2)$ is used, with $\xi = 0.7$ and $\omega_n = 40\omega_s$, where $\omega_s = 2\pi$ is the frequency of the input signal.

A comparison between the predicted responses and the corresponding experimental data is provided in Figure 3. The Bouc-Wen model predicts the force-displacement behavior of the damper well, and it possesses force-velocity behavior that also closely resembles the experimental data. Therefore, it is reasonable to believe that the Bouc-Wen model and the corresponding parameter identification method can predict the hysteretic behavior of the MRD accurately.

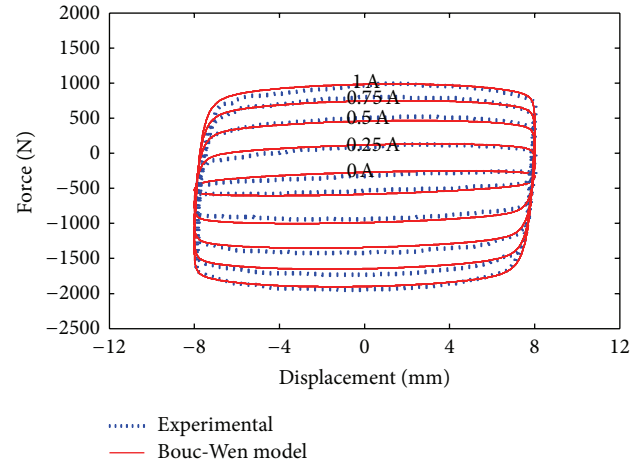

(a) Force versus displacement

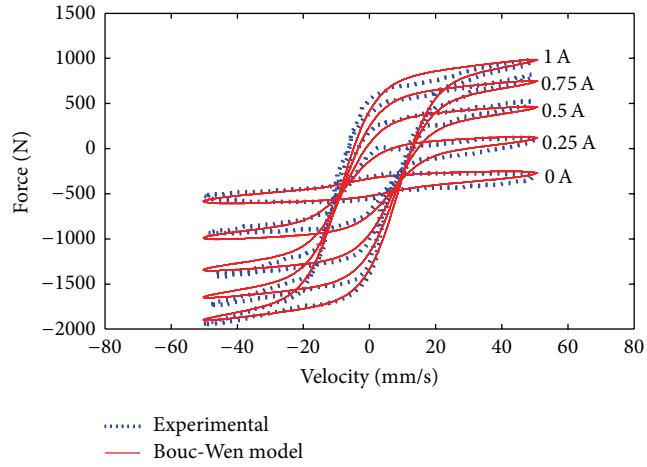

(b) Force versus velocity

Figure 3: Comparison between the predicted and experimentally obtained responses for the Bouc-Wen model under a 1 Hz sinusoidal excitation.

4. MRE Device

The MRE device, which is composed of two MREs, coil and two magnetic conductors, is shown in Figure 4. The size of the MRE device can be given by

$$r_1 = 3.5\,\text{mm}, \quad r_2 = 12.7\,\text{mm}, \quad r_3 = 17.7\,\text{mm}, \quad r_4 = 21.5\,\text{mm}, \quad l = 3\,\text{mm}. \tag{25}$$

According to (25), $r_2^2 - r_1^2 = r_4^2 - r_3^2$. Therefore, the areas of two MREs are equal, which can make the magnetic induction intensity of two MREs be consistent.

So the total area of MREs can be given by

$$A = \pi\left(r_2^2 - r_1^2\right) + \pi\left(r_4^2 - r_3^2\right) = 9.36 \times 10^{-4}\,\text{m}^2. \tag{26}$$

The middle hole with screw can play the roles of fixed and limited displacement.

The average values of tension/compression modulus and loss factor with current at different loading frequencies (1 Hz,

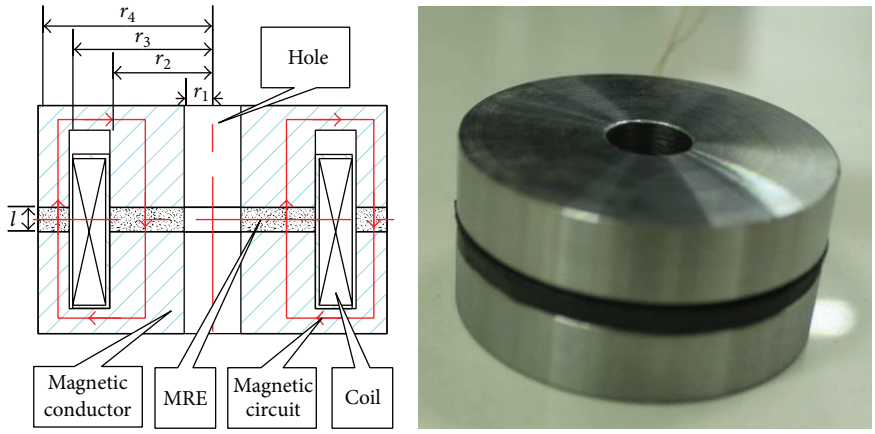

(a) Structure (b) Photograph

FIGURE 4: MRE device.

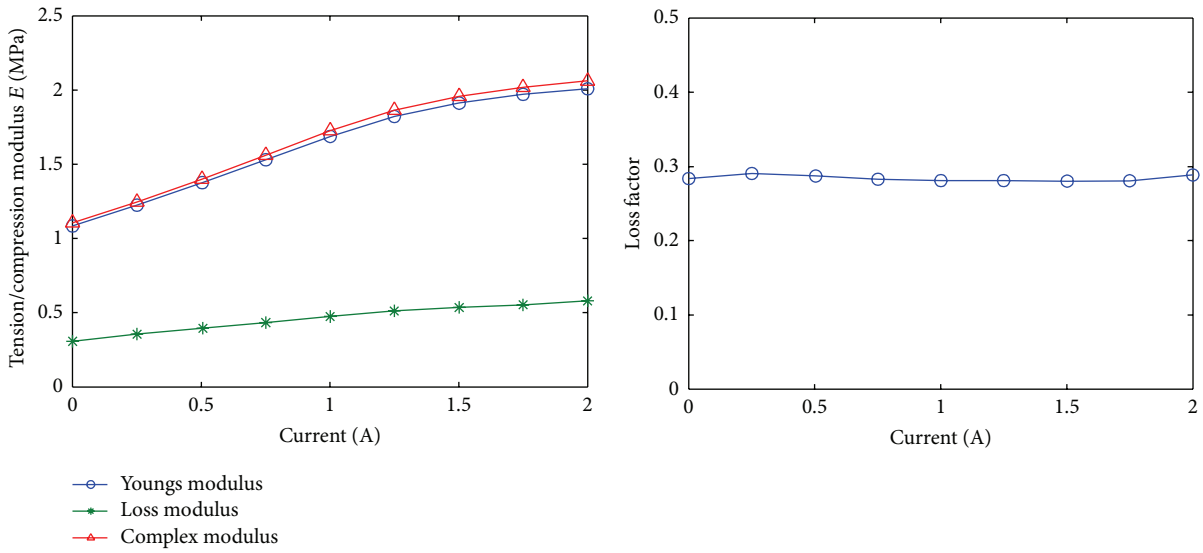

(a) Tension/compression modulus (b) Loss factor

FIGURE 5: Average values of the tension/compression modulus and loss factor with the various current at different loading frequencies (1 Hz, 10 Hz, 20 Hz, and 30 Hz).

10 Hz, 20 Hz, and 30 Hz) are shown in Figure 5. E represents the complex tension/compressive modulus, which can be expressed as

$$E = E' + iE'', \tag{27}$$

where E' is the storage modulus and E'' is the loss modulus. The loss factor η can be expressed as

$$\eta = \frac{E''}{E'}. \tag{28}$$

From Figure 5, we have

$$k_{\min} = E_{\min}\frac{A}{l} = 3.37 \times 10^5 \text{ N/m},$$
$$k_{\max} = E_{\max}\frac{A}{l} = 6.24 \times 10^5 \text{ N/m}, \tag{29}$$

where $E_{\min}$ and $E_{\max}$ are the minimum and maximum value of the storage modulus, respectively; $k_{\min}$ and $k_{\max}$ are the minimum and maximum value of the stiffness, respectively.

The stiffness and damping of the MRE device can be given by

$$k_{\text{MRE}} = k_{\min} + K(i), \qquad d_{\text{MRE}} = \frac{\eta k_{\text{MRE}}}{\omega}, \tag{30}$$

where $K(i)$ is a stiffness function of the efficient current i. Observing Figure 5, we have

$$K(i) = -0.1391i^2 + 0.7649i. \tag{31}$$

Figure 6 shows a single-DOF mass-damper-spring semi-active vibration control system composed of the MRE device and a mass. Let mass = 5 kg. The bode diagram of the system

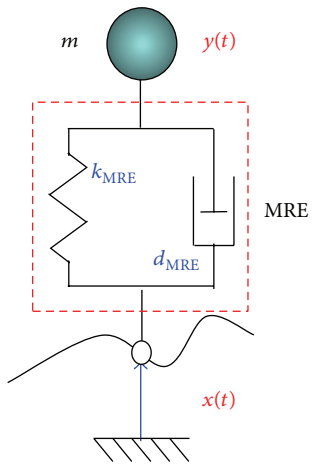

Figure 6: Single-DOF mass-damper-spring semiactive vibration control system.

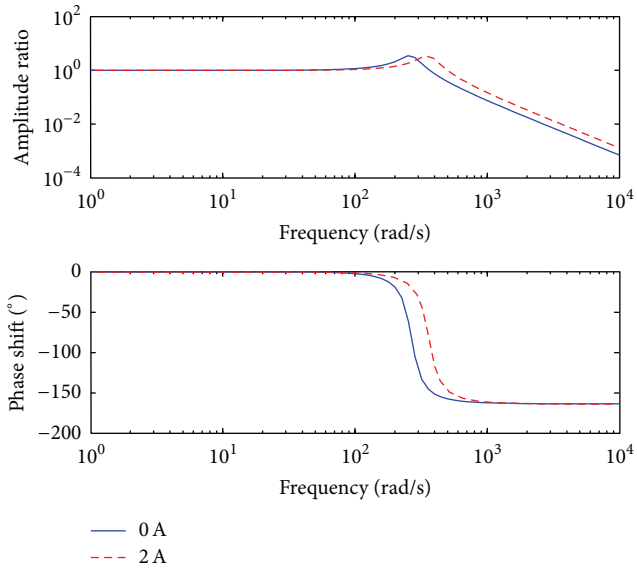

Figure 7: Bode diagram of the system shown in Figure 5 with the various applied current.

with the applied various current is shown in Figure 7. From Figure 7, the vibration characteristics of the system can be changed by the various currents. Therefore, the MRE device can reduce vibration when the semiactive vibration control is proposed.

5. Semiactive Vibration Control Strategy

According to (1), the state-space equation of the system can be given by

$$\dot{\mathbf{X}} = \mathbf{A}\mathbf{X} + \mathbf{B}f_{\mathrm{MRD}} + \mathbf{E}x_0, \qquad \mathbf{Y} = \mathbf{C}\mathbf{X}, \tag{32}$$

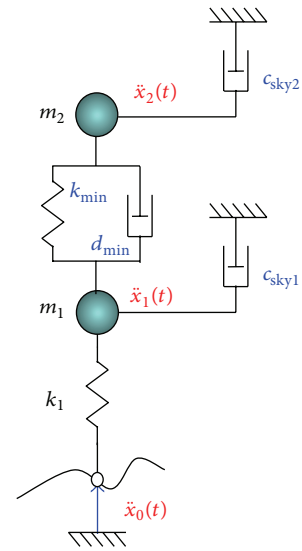

Figure 8: Sky-hook control model [16].

where

$$\mathbf{X} = \begin{bmatrix} x_1 \\ x_2 \\ \dot{x}_1 \\ \dot{x}_2 \end{bmatrix}, \qquad \mathbf{A} = \begin{bmatrix} \mathbf{0}_{2\times 2} & \mathbf{I}_2 \\ -\mathbf{M}_s^{-1}\mathbf{K} & -\mathbf{M}_s^{-1}\mathbf{C} \end{bmatrix},$$
$$\mathbf{B} = \begin{bmatrix} \mathbf{0}_{2\times 1} \\ \mathbf{M}^{-1}\Gamma \end{bmatrix}, \qquad \mathbf{E} = \begin{bmatrix} 0 \\ 0 \\ \mathbf{M}_s^{-1}\mathbf{K}_0 \end{bmatrix}, \qquad \mathbf{C} = \begin{bmatrix} 1 \\ 1 \\ 0 \\ 0 \end{bmatrix}. \tag{33}$$

The sky-hook control [10, 20, 21] is widely used semiactive vibration control. The sky-hook control model of the vibration control system is shown in Figure 8. From Figure 8 and according to (32), we have

$$f_{\mathrm{MRD}} = \begin{cases} F_{\max}, & \dot{x}_1(\dot{x}_1 - \dot{x}_0) \geq 0,\ F_{\max} < c_{\mathrm{sky1}}\dot{x}_1, \\ c_{\mathrm{sky1}}\dot{x}_1, & \dot{x}_1(\dot{x}_1 - \dot{x}_0) \geq 0,\ F_{\max} \geq c_{\mathrm{sky1}}\dot{x}_1, \\ 0, & \dot{x}_1(\dot{x}_1 - \dot{x}_0) < 0, \end{cases} \tag{34}$$

$$k_{\mathrm{MRE}} = \begin{cases} k_{\max}, & \dot{x}_2(x_2 - x_1) \geq 0, \\ & c_{\mathrm{sky2}}\dot{x}_2 > (x_2 - x_1)k_{\max}, \\ \dfrac{c_{\mathrm{sky2}}\dot{x}_2}{x_2 - x_1}, & \dot{x}_2(x_2 - x_1) \geq 0, \\ & c_{\mathrm{sky2}}\dot{x}_2 \leq (x_2 - x_1)k_{\max}, \\ k_{\min}, & \dot{x}_2(x_2 - x_1) < 0, \end{cases} \tag{35}$$

where c_{sky1} and c_{sky2} are the sky-hook damped coefficients.

Consider the actual dynamic responses of the system can be obtained by the sensors. The Bouc-Wen model of the MRD is computed in real time for the constant currents $i = 0, 0.1, \ldots, i_{\max D}$ A for the actual displacement and velocity. The corresponding estimated forces of the MRD can be obtained theoretically by calculation. Based on the estimated forces and the desired control force f_{MRD}, the control current i_{control} is derived by piecewise linear interpolation [12, 22]. Therefore, (34) can be rewritten as

$$i_{\mathrm{MRD}} = \begin{cases} i_{\max D} & \dot{x}_1\left(\dot{x}_1 - \dot{x}_0\right) \geq 0,\ i_{\mathrm{control}} > i_{\max D} \\ i_{\mathrm{control}} & \dot{x}_1\left(\dot{x}_1 - \dot{x}_0\right) \geq 0,\ i_{\mathrm{control}} \leq i_{\max D} \\ 0 & \dot{x}_1\left(\dot{x}_1 - \dot{x}_0\right) < 0, \end{cases} \tag{36}$$

where i_{MRD} is the actual control current of the MRD.

According to (30), (31), and (35), the actual control current of the MRE can be expressed by

$$i_{\mathrm{MRE}} = \begin{cases} i_{\max E}, & \dot{x}_2\left(x_2 - x_1\right) \geq 0, \\ & c_{\mathrm{sky2}}\dot{x}_2 > \left(x_2 - x_1\right) \\ & \quad \times \left(k_{\min} + K\left(i_{\mathrm{maxE}}\right)\right), \\ K^{-1}\left(\dfrac{c_{\mathrm{sky2}}\dot{x}_2}{x_2 - x_1}\right), & \dot{x}_2\left(x_2 - x_1\right) \geq 0, \\ & c_{\mathrm{sky2}}\dot{x}_2 \leq \left(x_2 - x_1\right) \\ & \quad \times \left(k_{\min} + K\left(i_{\mathrm{maxE}}\right)\right), \\ 0, & \dot{x}_2\left(x_2 - x_1\right) < 0, \end{cases} \tag{37}$$

where $K^{-1}(k)$ is the inverse function of $K(i)$, and its value range is $[0 \quad i_{\max E}]$; $i_{\max E}$ is the maximum control current of the MRE.

According to (36) and (37), the actual control currents of the MRD and the MRE can be obtained.

6. Experimental Implementation

In order to experimentally validate the proposed vibration control system and the semiactive vibration control strategy, the schematic and photograph of the experimental setup are shown in Figures 9(a) and 9(b), respectively. According to Figure 9, the experimental setup is composed of the proposed vibration control system, accelerometers (type: CA-YD-109B, range: 0–50 m/s^2, linearity: 99.8%), charge amplifier (type 5018, Kistler Corporation), current source (linearity: 99.2%), vibration table (type: MPA407/G334A, force range: 0–6000 kgf, frequency range: 0–2500 Hz, ETS Solutions Ltd), DSP (type: MS320F2812, TI Corporation), 12 bit A/D, 16 bit D/A, and data acquisition.

The acceleration responses of the mass 2 of the vibration control system with different control methods under a 10 Hz sinusoidal, 40 Hz sinusoidal, and nonperiodic acceleration excitations are shown in Figure 10. The uncontrolled method means that the input currents of both the MRD and the MRE are zero.

Table 1: Acceleration responses of the mass 2.

Vibration excitation	Control method	$\lvert a\rvert_{\max}$ (m/s^2)	E
10 Hz	Uncontrolled	10.13	5.34
	Control MRD	3.21	2.56
	Control MRD + MRE	2.67	1.69
40 Hz	Uncontrolled	19.5	9.25
	Control MRD	6.94	4.32
	Control MRD + MRE	6.31	2.92
Nonperiodical	Uncontrolled	29.6	10.25
	Control MRD	12.9	4.83
	Control MRD + MRE	9.26	3.58

The whole evaluation vibration acceleration response is defined as

$$E = \frac{1}{t}\sqrt{\int_0^t a^2(\tau)\,\mathrm{d}\tau}, \tag{38}$$

where $a(\tau)$ is the acceleration of the mass 2 in the time τ.

According to (38) and Figure 10, responses of the vibration control system with different control method are listed in Table 1. The acceleration responses of mass 2 dropped significantly with the semiactive control, which indicates the vibration control system with the semiactive control strategy is very effective in reducing the vibration. Interestingly, the control MRD can effectively reduce the peak acceleration responses but inspire some of the high-frequency vibrations. The MRE can not only marginally reduce the amplitude of the acceleration responses but can also play an important role in high-frequency vibration reduction. Therefore, MREs can be used to make up for the shortcomings of MRDs in vibration control system, which is consistent with the design idea in Section 2.

7. Conclusions and Future Scope

The vibration control system was put forward using the MRD and the MRE connected in series. In order to modeling the hysteresis of the MRD, the Bouc-Wen model and the corresponding parameter identification method were developed for the MRD. The role of the MRE was illustrated by an example of a single degree-of-freedom system. the semiactive vibration control strategy of the proposed vibration control system was proposed. To validate this new approach, experiments were conducted. The following conclusions can be drawn.

(1) The experiments results validate the proposed Bouc-Wen model and the corresponding parameter identification method can predict the hysteretic behavior of the MRD accurately.

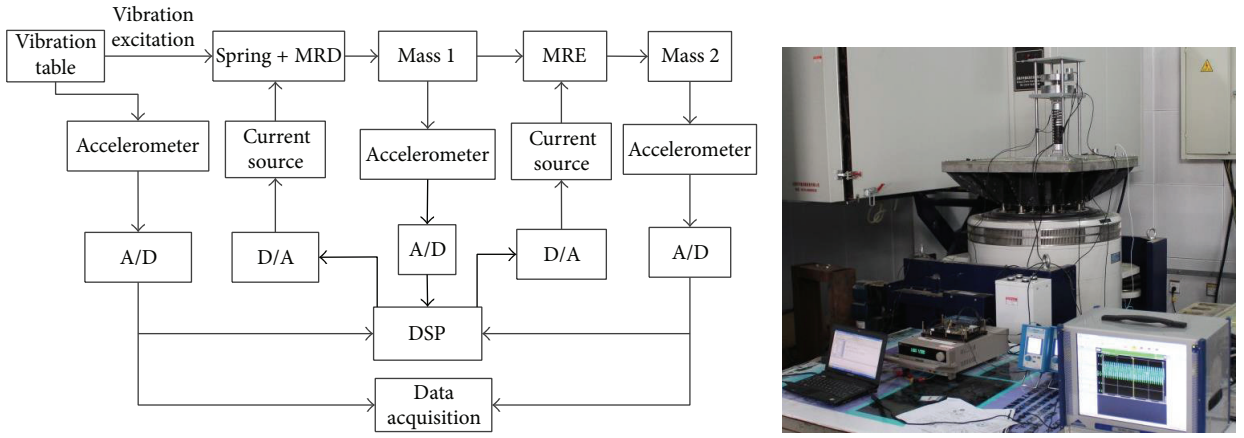

(a) Schematic diagram

(b) Photograph

Figure 9: Experimental setup.

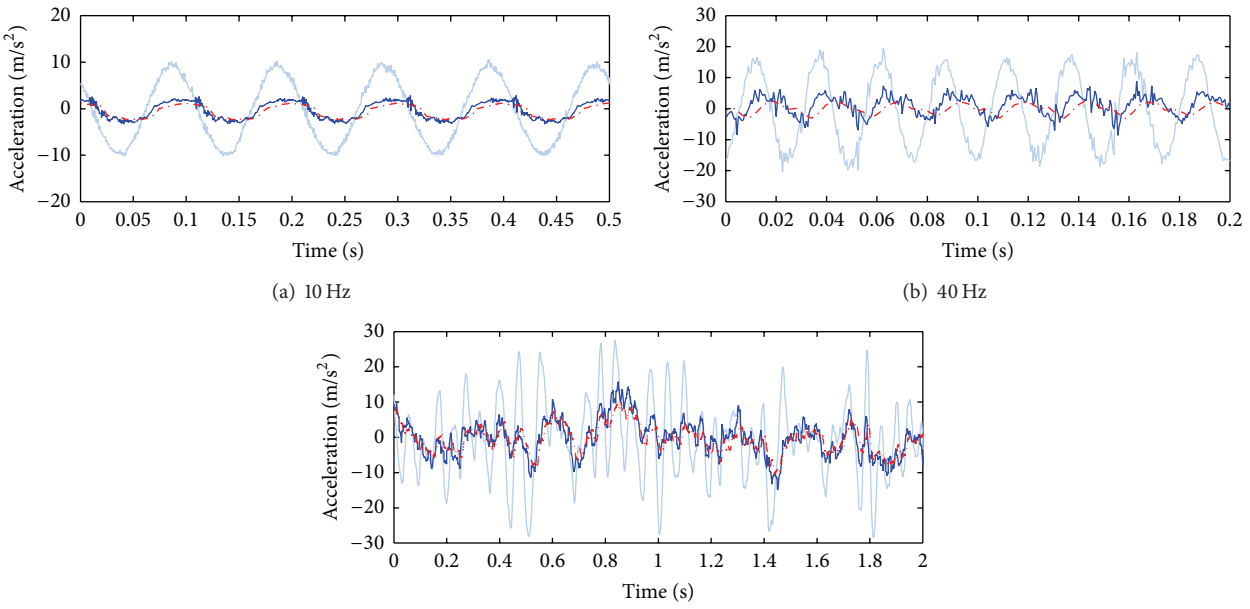

(a) 10 Hz

(b) 40 Hz

(c) Nonperiodical

Figure 10: Acceleration responses of the mass 2 with different control.

(2) The vibration control system with the semiactive control strategy is very effective in reducing the vibration.

(3) The MRD can reduce the large-range and low-frequency vibration and the MRE can reduce the small-range and high-frequency vibration.

According to the above conclusions, the future work involves.

(1) researching their applications, such as suspension system

(2) researching the vibration control system using the MRD and the MRE connected in parallel.

Conflict of Interests

The authors declare that there is no conflict of interests regarding the publication of this paper.

Acknowledgment

The authors wish to acknowledge the financial support by Natural Science Foundation of China (NSFC Grant no. 61304137).

References

[1] N. K. Chandiramani and S. P. Purohit, "Semi-active control using magnetorhelogical dampers with output feedback and distributed sensing," *Shock and Vibration*, vol. 19, no. 6, pp. 1427–1443, 2012.

[2] Y.-K. Wen, "Method for random vibration of hysteretic systems," *ASCE Journal of Engineering Mechanics Divison*, vol. 102, no. 2, pp. 249–263, 1976.

[3] B. F. Spencer Jr., S. J. Dyke, M. K. Sain, and J. D. Carlson, "Phenomenological model for magnetorheological dampers," *Journal of Engineering Mechanics*, vol. 123, no. 3, pp. 230–238, 1997.

[4] A. Dominguez, R. Sedaghati, and I. Stiharu, "A new dynamic hysteresis model for magnetorheological dampers," *Smart Materials and Structures*, vol. 15, no. 5, pp. 1179–1189, 2006.

[5] L. X. Wang and H. Kamath, "Modelling hysteretic behaviour in magnetorheological fluids and dampers using phase-transition theory," *Smart Materials and Structures*, vol. 15, no. 6, pp. 1725–1733, 2006.

[6] R. Jiménez and L. Álvarez-Icaza, "LuGre friction model for a magnetorheological damper," *Structural Control and Health Monitoring*, vol. 12, no. 1, pp. 91–116, 2005.

[7] C. Sakai, H. Ohmori, and A. Sano, "Modeling of MR damper with hysteresis for adaptive vibration control," in *Proceedings of the 42nd IEEE Conference on Decision and Control*, pp. 3840–3845, Maui, Hawaii, USA, December 2003.

[8] Z.-D. Xu and Y.-P. Shen, "Intelligent bi-state control for the structure with magnetorheological dampers," *Journal of Intelligent Material Systems and Structures*, vol. 14, no. 1, pp. 35–42, 2003.

[9] S. J. Dyke, B. F. Spencer Jr., M. K. Sain, and J. D. Carlson, "Modeling and control of magnetorheological dampers for seismic response reduction," *Smart Materials and Structures*, vol. 5, no. 5, pp. 565–575, 1996.

[10] S. Frey, K. Groh, and A. Verl, "Semi-active damping of drive systems," *JVC/Journal of Vibration and Control*, vol. 19, no. 5, pp. 742–754, 2013.

[11] R. S. Prabakar, C. Sujatha, and S. Narayanan, "Optimal semi-active preview control response of a half car vehicle model with magnetorheological damper," *Journal of Sound and Vibration*, vol. 326, no. 3-5, pp. 400–420, 2009.

[12] F. Weber, "Bouc-Wen model-based real-time force tracking scheme for MR dampers," *Smart Materials and Structures*, vol. 22, no. 4, Article ID 045012, 12 pages, 2013.

[13] G. Y. Zhou and F. Weber, "Complex shear modulus of a magnetorheological elastomer," *Smart Materials and Structures*, vol. 13, no. 5, pp. 1203–1210, 2004.

[14] Z. Rigbi and L. Jilkén, "The response of an elastomer filled with soft ferrite to mechanical and magnetic influences," *Journal of Magnetism and Magnetic Materials*, vol. 37, no. 3, pp. 267–276, 1983.

[15] M. R. Jolly, J. D. Carlson, and B. C. Muñoz, "A model of the behaviour of magnetorheological materials," *Smart Materials and Structures*, vol. 5, no. 5, pp. 607–614, 1996.

[16] A. Preuont, *Vibration Control of Active Structures*, Kluwer Academic Publishers, 2002.

[17] W. Zhu and D.-H. Wang, "Non-symmetrical Bouc-Wen model for piezoelectric ceramic actuators," *Sensors and Actuators A: Physical*, vol. 181, pp. 51–60, 2012.

[18] C.-J. Lin and S.-R. Yang, "Precise positioning of piezo-actuated stages using hysteresis-observer based control," *Mechatronics*, vol. 16, no. 7, pp. 417–426, 2006.

[19] A. Rodríguez, N. Iwata, F. Ikhouane, and J. Rodellar, "Model identification of a large-scale magnetorheological fluid damper," *Smart Materials and Structures*, vol. 18, no. 1, Article ID 015010, 2009.

[20] C. Collette and A. Preumont, "High frequency energy transfer in semi-active suspension," *Journal of Sound and Vibration*, vol. 329, no. 22, pp. 4604–4616, 2010.

[21] C. Spelta, S. M. Savaresi, F. Codecà, M. Montiglio, and M. Ieluzzi, "Smart-bogie: semi-active lateral control of railway vehicles," *Asian Journal of Control*, vol. 14, no. 4, pp. 875–890, 2012.

[22] F. Weber, "Semi-active vibration absorber based on real-time controlled MR damper," *Mechanical Systems and Signal Processing*, vol. 46, pp. 272–288, 2014.